



**Cesium Lead Bromide Semiconductor Radiation Detectors:
Crystal Growth, Detector Performance and Ionic
Polarization**

Journal:	<i>Journal of Materials Chemistry C</i>
Manuscript ID	TC-ART-04-2022-001679.R1
Article Type:	Paper
Date Submitted by the Author:	05-Jul-2022
Complete List of Authors:	Toufanian, Reyhaneh; CapeSym Inc, R&D Swain, Santosh; CapeSym Inc, R&D Becla, Piotr; CapeSym Inc, R&D Datta, Amlan; CapeSym Inc, R&D Motakef, Shariar; CapeSym Inc, R&D

ARTICLE

Cesium Lead Bromide Semiconductor Radiation Detectors: Crystal Growth, Detector Performance and Polarization

Reyhaneh Toufanian,^a Santosh Swain,^a Piotr Becla,^a Shariar Motakef^{†a} and Amlan Datta,^{*†a}

Received 00th January 20xx,
Accepted 00th January 20xx

DOI: 10.1039/x0xx00000x

Cesium lead bromide (CsPbBr₃) is an upcoming semiconductor radiation detector that has the potential to match the detection properties of cadmium zinc telluride (CZT) and thallium bromide (TlBr). In this paper, we report on CsPbBr₃ gamma detectors with an uncorrected energy resolution of 2% at 662keV with Photopeak-to-Compton ratios as high as 14.3 and hole mobility-lifetime products ($\mu\tau_h$) as high as 1.7×10^{-2} cm²/V. Furthermore, we demonstrate that the processes employed for material purification and crystal growth of high-performing devices are scalable and large (up to 65mm in diameter) ultrahigh purity CsPbBr₃ crystals have been successfully grown. Using optimized growth conditions and detector fabrication processes, we were able to mitigate the polarization problem where it was revealed that the polarization process is highly dependent on the crystal quality and the electric field direction with respect to the orientation of the crystal.

A. Introduction

Spectroscopic gamma detectors have numerous applications spanning from homeland security to medical imaging.¹ Semiconductor-based gamma detectors can provide unmatched energy resolution (ER) as high as 0.1% at 662 keV as in the case of cooled High Purity Ge (HPGe). Cadmium Zinc Telluride (CZT) radiation detectors are currently the only commercially available room-temperature semiconductor detectors, with their superior spectral resolution approaching the performance of cooled HPGe detectors. The persistently high price and the slow increase in the size of these detectors, however, reveal a low production yield. Two halide semiconductor detector materials, thallium bromide (TlBr) and cesium lead bromide (CsPbBr₃) have been demonstrated to have a spectral resolution performance similar to that of CZT.² Of these, TlBr has been under development for a relatively long time and has recently emerged as a strong potential replacement for high-ER CZT detectors.³ CsPbBr₃ and other perovskite semiconductors, on the other hand, are rapidly emerging as strong competitors to TlBr and CZT, both in terms of innate properties and potentially lower production cost.

Lead (Pb) halide perovskites with a APbX₃ formula (where A⁺ = cesium (Cs) or methylammonium (CH₃NH₃ or MA) and X⁻ = chlorine (Cl), bromine (Br) or iodine (I)) are highly attractive as room temperature gamma-ray detectors. Table 1 compares their properties with those of CZT and TlBr. These perovskites have a high γ -ray attenuation coefficient owing to the presence of Pb, Figure 1. In these materials, the hole mobility-lifetime

product ($\mu\tau_h$) is generally considered to be higher than the electron mobility-lifetime product ($\mu\tau_e$),^{4,5} The energy resolutions of planar detectors from the melt- and solution-grown CsPbBr₃ crystals at 662 keV are 3.8% and 5.5%, respectively.^{4,5} The best ER value reported for MAPbBr_{2.94}Cl_{0.06} is 6.5%, with typical values of 12.5%.⁶ Pixelated radiation detectors fabricated from melt-grown 8x8x5 mm³ CsPbBr₃ have been recently reported to exhibit a high ER of 1.4% at 662 keV, similar to ~1% value reported for TlBr detectors and close to the 0.7% values reported for CZT.^{7,8}

The perovskite detectors have the added advantage of low charge trap density and high defect tolerance.^{4,5} For the successful commercialization of these perovskite-based gamma detectors, the crystal growth process must be scaled up to produce large diameter crystals while maintaining the excellent charge carrier properties is crucial. Although solution growth is a very attractive low capital cost technique with immense potential for the development of low-cost gamma detectors, currently, there are no published results that can conclusively demonstrate its applicability towards repeatable production of gamma detectors with consistently high ER. The melt growth techniques have produced the most reliable results, albeit on relatively small scales.⁹ Due to the relatively lower resistivity of the perovskite materials, these detectors are typically fabricated using Schottky contacts.¹⁰ Although there have been studies of ionic migration in MAPbBr₃ semiconductors, the underlying mechanisms of performance degradation in CsPbBr₃ gamma detectors are not discussed in the literature.^{11,12} In the case of TlBr, circumventing this challenge was a crucial factor in its commercialization.^{13–16}

Our study demonstrates the scale-up of the CsPbBr₃ crystal growth technology using the vertical Bridgman (VB) melt growth process. The excellent spectroscopic properties of the detectors were used as the success metric. The challenge of ionic migration in this material has not been studied before.

^a CapeSym Inc, 6 Huron Drive, Natick, MA 01760.

* Corresponding Author (Email: datta@capecsym.com)

† Same contribution by the authors.

Electronic Supplementary Information (ESI) available: [details of any supplementary information available should be included here]. See DOI: 10.1039/x0xx00000x

Here, we present a comprehensive model of the ionic migration problem in this material and illustrate a potential solution.

Table 1. Material properties for semiconductor radiation detectors.

Material (Growth Technique)	Density ₃ (g/cm ³)	Z _{eff}	E _g (eV)	ρ (Ω.cm)	μ _e (cm ² /Vs)	μ _h (cm ² /Vs)	(μτ) _e (cm ² /V)	(μτ) _h (cm ² /V)
CZT	5.78	50	1.57	10 ¹⁰	1000	100	~1x10 ⁻²	~1x10 ⁻³
TlBr	7.56	74.8	2.68	10 ¹¹	30	4	~1x10 ⁻²	4x10 ⁻⁴
CsPbBr ₃ (Melt, Literature)	4.85	65.9	2.28	10 ⁹	63	52	>8x10 ⁻⁴	~8x10 ⁻³
CsPbBr ₃ (Melt, CapeSym)	4.85	65.9	2.28	10 ¹⁰	-	-	-	~1x10 ⁻²
CsPbBr ₃ (Solution, Literature)	4.85	65.9	2.28	-	181	56	7x10 ⁻⁴	2x10 ⁻³

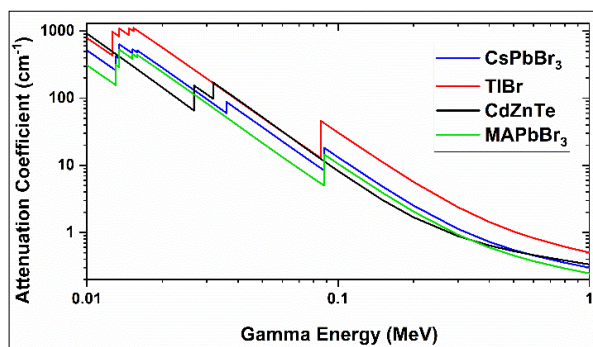


Figure 1. High mass attenuation coefficient versus gamma energy for several semiconductor radiation detectors.

B. Results and discussion

In this section, we demonstrate the precursor purification and crystal growth process for production of detector-grade CsPbBr₃ single crystals, gamma spectroscopy and charge carrier properties of the detectors, and the ionic polarization phenomena observed in these halide perovskite detectors.

I. Purification and Crystal Growth of CsPbBr₃

We explored various starting material purification approaches, multiple growth and post-growth cooling protocols, as well as composition variations aimed at enhancing electro-optical and structural quality of the detectors, and scaled up the size of grown crystals. The zone refining technique was used for purification of the precursors. The growth and post-growth conditions, such as temperature gradient and cooling rates, were varied to attain the best crystalline quality. Fifteen purification experiments and 25 vertical Bridgman (VB) CsPbBr₃ crystal growth runs were completed. In addition, two Czochralski and 22 solution growth experiments were conducted, showing the versatility of CsPbBr₃ and viability of these low-cost, high-yield growth approaches. In this paper we report only on the VB grown crystals. The largest VB-grown CsPbBr₃ crystal was 65mm in diameter and 75mm in height. The optimized melt-grown crystals showed resistivities on the order of 1x10¹⁰ Ω.cm. Devices fabricated from these crystals demonstrated stable gamma response with high (μτ)_h. The details of the electronic and spectroscopic properties of the devices made from these crystals are given in section B.II and B.III.

The starting materials were 99.999% purity CsBr and PbBr₂ beads acquired from Sigma Aldrich (EMD performance materials). The same batch of the precursors was used for all growths to maintain repeatability in the crystal growth experiments. These ultrahigh purity beads were used to form the CsPbBr₃ compound and were further purified using the zone refining (ZR) technique. Sublimation can also be used as a purification process for low-temperature halide materials. However, as stoichiometric shifts can be uncertain during sublimation, this process was not used.

For ZR purification, two-zone refiners were used in a single pass providing high throughput. Figure 2 shows a typical zone refined crystal. During zone refining, depending on their respective solubilities and segregation coefficients, impurities segregate towards the two ends of the crystal. The region towards the end of the zone refining pass appears to be darker than the central region. After successfully segregating out the impurities by zone refining, we used the bright orange part of the crystal for VB growths. The discarded regions are shown by black "X"es in Figure 2. ZR materials subjected to various numbers of passes, from 7 up to 75 passes, were used in different VB growths. These crystals produce high resistivity (10⁹-10¹⁰ Ω.cm) detectors. As discussed later, the impurity analysis performed on a ZR CsPbBr₃ crystal shows the excellent effectiveness of this purification process. This is also evident from the color of the as-grown crystals (Figure 3). ZR process eliminated all metal impurities from the precursor material, thereby minimizing defect centers in the CsPbBr₃ bandgap which are generally detrimental to the charge collection properties of the semiconductor detectors. The best performing crystals were fabricated from crystals grown from purified by 75 zone refining passes which demonstrates the positive effects of impurity elimination on the material properties.



Figure 2. A typical zone refined crystal showing the region that is discarded before using it as charge material for a VB growth.

VB growths are performed in a two-zone vertical Bridgman furnace, by either translating the furnace or the ampoule at a rate of 0.6 mm/hr. Crystals are grown under various growth conditions, cooling rates, and compositions intended to improve crystal quality and properties. Furnaces equipped with heat pipes were employed, providing a well-defined temperature gradient at the growth interface and uniform temperature along the ingot length during post-growth cooling.

CsPbBr₃ goes through two distinct phase transitions at 130°C and 88°C:



Therefore, the crystals are very sensitive to the cooldown rates, which can degrade the crystalline quality and detector properties as a result of changes in the crystal structure and lattice constants. We tested various cooldown rates between 1°C/hr to higher than 25°C/hr through the phase transition temperature with a few crystals being held near the upper transition temperature (130°C) for 168 hours. Using powder X-ray diffraction (XRD), the crystal structure of

a series of samples was determined as orthorhombic, consistent with the low-temperature stable phase (Figure S2).



Figure 3. As-grown CsPbBr₃ crystals before and after optimization of the purification process.

The growth of small crystal boules is useful for understanding and optimizing the material properties, and the majority of the published research on CsPbBr₃ makes use of crystals grown in small diameters. For large volume commercial crystal growth, it is important to retain the quality of the crystals. Maintaining a stable growth interface, compositional uniformity and single crystalline qualities pose challenges to the boule size scale-up. We have achieved a 5-fold increase in crystal size while maintaining high quality crystal properties (Figure 4).



Figure 4. 65 mm diameter CsPbBr₃ single crystal, largest ever produced. The inhomogeneities in the crystal color are limited only to the surface.

Glow discharge mass spectrometry (GDMS) elemental analysis was performed on the middle section samples from the VB-grown crystals. The GDMS analysis revealed that the impurities comprised small amounts of Ag, Ca, K, Na, and Si (Figure 5) along with Cl. The origin of Cl is believed to be contamination of the halide precursor synthesis process at the vendor facility. We have also observed that slight Cl-doping is advantageous for obtaining stable spectroscopic properties of the CsPbBr₃ based gamma detectors. The source of Si impurities is the quartz ampoules themselves. In a representative CsPbBr₃ crystal, the total metallic impurities that affect the bandgap properties of the detectors was approximately 2ppm. The effect of high purity is clearly visible from the high μ_{τ} values and the excellent gamma response from the CsPbBr₃ detectors.

The brittle nature of the CsPbBr₃ crystals results in microcracks on the surface of the detector that propagate inwards if not properly handled. In order to obtain CsPbBr₃ detectors from these crystals,

the detector fabrication process was carefully optimized (see experimental section). The resulting detectors were free of microcracks, etch pits, and any other types of microcrystalline defects.

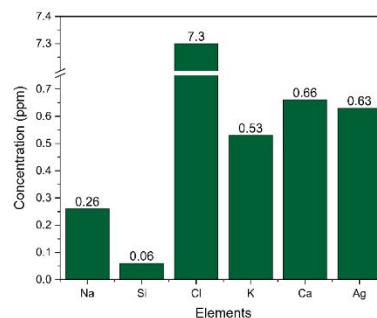


Figure 5. Impurities present in the CsPbBr₃ VB grown crystals using ZR purified precursors. The total impurity was below 2ppm in most of the crystals.

Selection of contacts for CsPbBr₃ detectors is, to a large extent, driven by the need to reduce the dark current in these devices. The conduction band minimum and valence band maximum in CsPbBr₃ are at -3.3 and -5.6 eV, respectively. Hole and electron mobilities in this material are similar, unlike that of CZT where the electron mobility is roughly ten times higher than hole mobility. The collection of holes, in contrast to the collection of electrons in CZT, avoids charge trapping issues resulting in higher energy resolution. Thus, to achieve both low dark current values and hole collection, it is necessary to select a contact material with a low work function to form a high Schottky barrier under reverse potential. We tested a number of contact materials in this study. Table 2 lists the contacts used for detector fabrication from various crystals. An energy band diagram of CsPbBr₃ and different metal contacts can be found in Figure S1. Au, In, Cr, Bi, Pb, SnO₂, and Se contacts were deposited using thermal evaporation, with a thickness of ~ 100 nm. Pt contacts were deposited using sputtering. Ga contacts were prepared by brushing the liquid metal to the surface of the sample. A barrier of 0.8-0.9 eV was measured in our devices with Ga contacts. In addition to Ga, a eutectic Ga/In (EGaIn) contact composed of 75 wt% Ga and 25 wt% In was also tested. The EGaIn contact provides better wetting properties to the surface of the semiconductor than the pure Ga metal.¹⁷ However, it was observed that for long-term applications, the Ga-based contacts corrode the CsPbBr₃ surface by forming a bimetallic alloy resulting in a significant increase in detector noise. Pb-based contacts were specifically designed for reducing the dark current noise and polarization of the detectors. The results of the Pb-contact study will be published elsewhere. We used the Au/In electrode structure for all of our experiments.

Table 2. Contact materials used in this study and their work functions.

Composition	Work Function (eV)	Electrode
Au	5.10-5.47	Cathode
Pt	5.12-5.93	Cathode
Se	5.9	Cathode
In	4.09	Anode
Ga	4.32	Anode
Cr	4.5	Anode
Bi	4.31	Anode

Pb	4.25	Anode
Sn	4.42	Anode

B. Gamma Spectroscopy with CsPbBr₃

Planar and pixelated CsPbBr₃ gamma detectors were fabricated from the large crystal boules. An example of an 18mm x 18mm x 6mm CsPbBr₃ pixelated detector is shown in Figure 6. The gamma response of these detectors was measured using a custom-designed preamplifier and pulse processing electronics. For obtaining high ER, the centroid position of the gamma response should not shift with time. This is only possible with detectors that do not demonstrate polarization problems. In detectors with polarization, the 662keV centroid shifts within minutes of operation (shown later in the paper), rendering them unusable for field applications. However, we have overcome this problem and obtained stable 662keV responses. A typical gamma response obtained from a stable pixelated (one pixel with a guard-ring) is shown in Figure 7. ER as low as 2% was achieved without any digital correction. In addition, the Compton-to-photopeak ratios are as high as 14.3. This is the first report of such a high Compton-to-photopeak ratio using CsPbBr₃ detectors that were obtained without any digital correction. The excellent performance of these detectors can be attributed to the efficient charge carrier properties. The next step of this study is bump-bonding of the pixelated detectors to electronic substrates for the development of radiation detection equipment such as RIID based on CsPbBr₃ detectors.

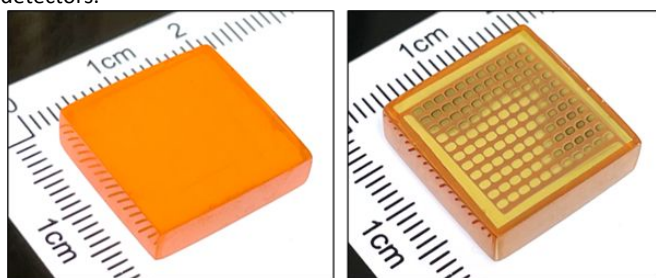


Figure 6. Polished CsPbBr₃ single sensor with dimensions 18mm x 18mm x 6mm (left) and a pixelated detector fabricated using that sensor (right).

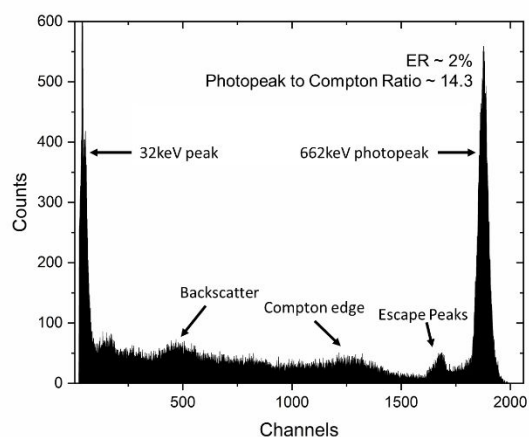


Figure 7. ¹³⁷Cs response from a CsPbBr₃ planar detector with guard-ring showing a 662 keV energy resolution of 2% at a bias of 350 volts.

C. Hole Mobility Lifetime ($\mu\tau$) Product of CsPbBr₃ Detectors

The $\mu\tau$ calculations were made according to the simplified single carrier Hecht equation using a ¹³⁷Cs gamma source. These calculations were based on the intensity of the output signal of the preamplifier at different detector bias voltages as reported by others.^{18,19} The amplitude of the transient pulse extracted from the preamplifier, which is proportional to the collected induced charge, was used for the determination of charge collection properties. The averaged pulse height was measured and used for Hecht fitting. The mobility was estimated from the rise time of transient pulses. Due to polarization in the unoptimized detectors which resulted in shifts in the preamplifier pulse amplitudes (and the peak channel) over time, measurement of $\mu\tau_h$ was not possible. We only measured the $\mu\tau_h$ values for the stable detectors. The best $\mu\tau_h$ value measured was $1.7 \times 10^{-2} \text{ cm}^2/\text{V}$ (Figure 8), with values as low as $2.3 \times 10^{-3} \text{ cm}^2/\text{V}$ also measured. The excellent $\mu\tau_h$ values allow the fabrication of thick detectors. The observed variations in $\mu\tau_h$ values reflect the local inhomogeneities in the crystals, which are related to variations in crystalline and chemical defects.

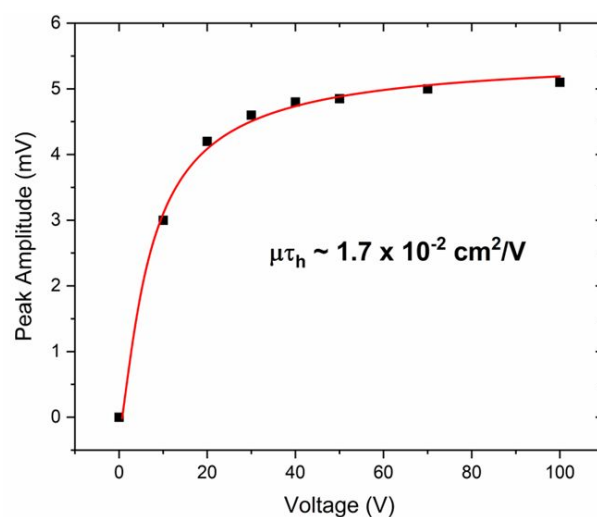


Figure 8. The best mobility-lifetime product for hole carriers obtained using a stable CsPbBr₃ detector. The thickness of the detector was 2mm.

D. Polarization Phenomena in CsPbBr₃ Detectors

CsPbBr₃ detectors exhibit polarization, a time-dependent degradation in ER under bias. In semiconductor detectors, the models of polarization that explain the available experimental data, attribute polarization to factors such as halide ion migration and slow detrapping of charge carriers at the interfaces under applied bias.²⁰ The electromigration of halide ions in halide semiconductors has been previously observed and extensively studied in semiconductors such as TlBr, where electromigration of Br⁻ ions and their subsequent chemical reaction with the contact metal result in rapid performance deterioration of the detector and its failure.^{16,21} The observed polarization effects in CsPbBr₃ semiconductors are different. Here, both the Cs⁺ and Br⁻ ions are mobile and appear to contribute to the polarization effects.²² Also, the deterioration of the contact metals, suggesting their reaction with the electro-migrating species, is far less pronounced when compared to TlBr. Polarization in CsPbBr₃ was first evidenced by the shift in channel number during gamma

spectroscopy measurements upon continuous bias application. This shift was later correlated to a change in the I-V characteristics of the detectors.

In order to quantify the polarization effects for gamma spectroscopy, we performed stability tests where γ -response measurements were taken approximately every 5 minutes under identical conditions of gain, shaping time, and continuous application of voltage. As depicted in Figure 9, a continuous shift of the photopeak to lower channels was observed under constant experimental conditions.

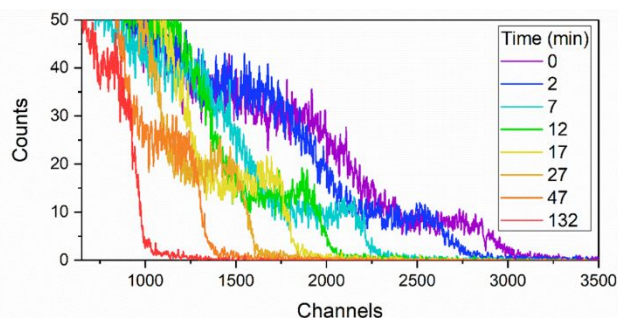


Figure 9. Evolution of the gamma response of an unstable CsPbBr₃ detector upon steady application of bias.

Interestingly, this phenomenon is reversible and repeatable. Once the application of bias is halted for a few hours, the photopeak returns to its original position, and the same trend is observed with the repeated application of bias on a similar time scale. The data in Figure 10 shows the shifts in the centroid position with time for the same detector repeatedly biased and turned off in regular intervals.

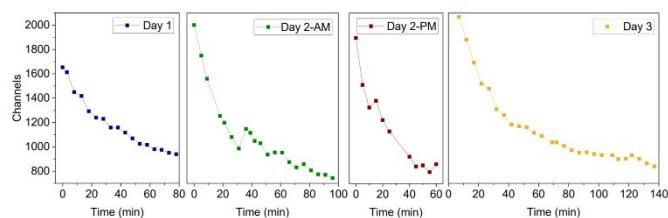


Figure 10. Recovery in the 662 keV gamma centroid positions due to reversible ionic polarization phenomena in an unstable CsPbBr₃ detector.

The shifts in the current-voltage properties were also periodically monitored to gain insight into the polarization phenomena of the CsPbBr₃ detectors. It was observed that the Schottky character of the semiconductor-to-metal junction changed over time depending on the direction of the applied bias. Figure 11 shows the changes in the schottky behavior along with the different relevant biasing conditions. After the fresh device was biased for an hour for spectroscopic testing, the Schottky current is highly denounced due to the lowering of the electric field inside the detector. Once the bias is reversed for an hour, the electric field slightly recovers and the Schottky current goes up. After additional time in reverse bias, the current surpasses the original value indicating polarization in the opposite direction. These changes, along with the shifts in the position of the photopeak is correlated to dominant defects in CsPbBr₃, mainly Pb_{Br} and Br_{Pb} substitutions.²³

As a solution to this polarization phenomenon, the biasing direction with respect to the crystallographic planes of the CsPbBr₃ crystals

was deemed extremely important. To investigate the dependence of polarization within the bulk of the semiconductor on the orientation of the crystallographic plates relative to the direction of the applied electric field, we fabricated detectors by sectioning the crystal in both parallel and perpendicular growth directions. Figure 12 shows an image of the CsPbBr₃ crystal and is marked with perpendicular (area 1) and parallel (area 2) samples. Detectors are typically fabricated using sections of the boule cut in a direction perpendicular to the crystal growth direction. However, the detectors fabricated from the parallel direction demonstrated stable γ -response peaks under varying biases up to 1000 V.

The parallel detectors were fabricated using our usual fabrication techniques. In order to demonstrate the stable performance of these detectors, we applied different electric fields and monitored the shifts in the 662keV centroid. The detector was continuously kept under bias, starting from a -700V bias, and demonstrated stability for 60 minutes. The bias was then lowered to -100V and finally raised to 1000V. The sample showed stable photopeaks for the entire duration of this experiment under varying applied biases, Figure 13. In contrast, the perpendicular detector from the same crystal shows a rapidly changing peak position. This difference may be attributed to orientation-dependent migration barriers, diffusion rates of migrating ions, surface defect density, and Schottky contact quality. Differences in the linear atomic density within the lattice structure result in varying diffusion rates and results in anisotropic electronic properties in the bulk crystal. By fabricating detectors from samples sectioned parallel to the crystal growth direction, stable high ER photopeaks were obtained, as shown in Figure 7.

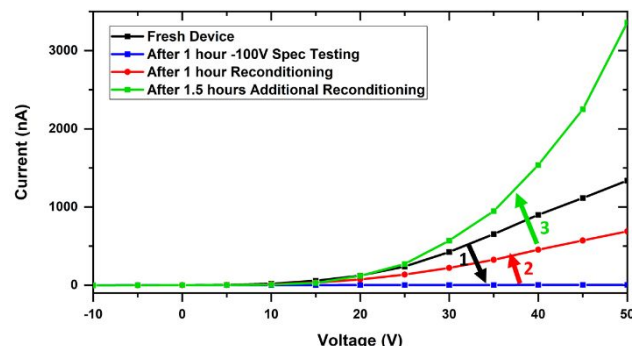


Figure 11. Changes in the Schottky current before and after reconditioning a detector, showing the reversible behavior of the polarization phenomena that results in the disappearance of the Schottky behavior of the CsPbBr₃ detectors with time.

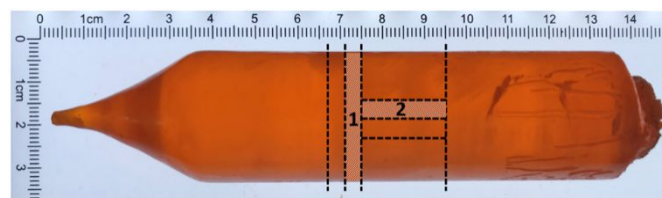


Figure 12. Image of a representative CsPbBr₃ crystal and schematic representation of the sectioning directions of samples for the fabrication of detectors.

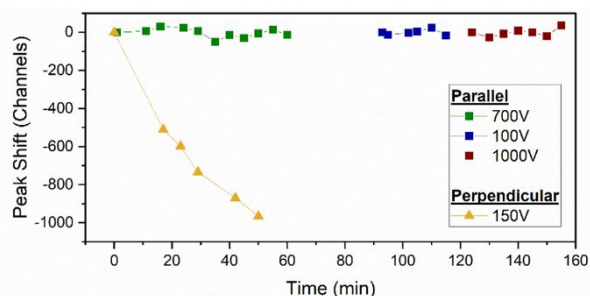


Figure 13. Stability of the gamma spectrum photopeak position of detectors fabricated from parallel and perpendicular cuts of the CsPbBr₃ crystal.

Experimental Section

CsPbBr₃ crystals were grown by the vertical Bridgman technique from zone refined material. The crystals were cut into 3 mm thick sections. The samples were rinsed with acetone prior to polishing for the complete removal of residual oil and were prepared by consecutive polishing on SiC polishing pads (600, 800, and 1200 mesh) to the desired thickness (~1-2.5 mm). Chemo-mechanical etching using a solution of DMSO and IPA on ultrapolish pads, which minimized the formation of etch pits and resulted in the formation of a defect-free surface. After a smooth surface was obtained, samples were thoroughly rinsed with acetone to remove the residual etchant and dried in ambient conditions prior to contact deposition. Au and In contacts were deposited by thermal evaporation, with a thickness of ~100 nm. Devices were stored in air without any encapsulation. I-V characteristics were measured under dark conditions using a Keithley 617 programmable electrometer.

The energy resolution (ER) of a characteristic peak was calculated using the following equation: FWHM/(peak channel number) × 100%. The $\mu\tau$ was calculated using the simplified single carrier Hecht

equation: $\eta = \frac{Q}{Q_0} = \mu\tau \frac{V}{d^2} (1 - e^{-\frac{d^2}{\mu\tau V}})$, where η is the charge collection efficiency, Q and Q_0 the maximum and theoretical saturated channel numbers of the photopeak/shoulder, respectively, V is the applied voltage, and d is the detector thickness.

Conclusions

We demonstrated stable high resolution ~2% ER in Schottky-type Au/CsPbBr₃/In detectors using processes adopted for commercial bulk crystal growth. I-V and spectroscopic characterization of the detectors revealed that the polarization process is reversible, and longer term stability could be achieved by suitable choice of fabrication and measurement conditions, which shows prospects for commercial success of this material in gamma spectroscopy and X-ray imaging.

Author Contributions

The manuscript was written through contributions of all authors. All authors have given approval to the final version of the manuscript. AD and SM conceptualized and directed this study. SS and AD performed the CsPbBr₃ crystal growths. AD, RT and PB characterized the CsPbBr₃ detectors.

Conflicts of interest

There are no conflicts to declare.

Acknowledgements

This research was sponsored by the National Nuclear Security Administration within US Department of Energy under competitively funded SBIR contract number DE-SC0020900. The content of this paper does not necessarily reflect the position of the US federal government, and no official endorsement should be inferred.

References

- Liu F, Wu R, Wei J, et al. Recent Progress in Halide Perovskite Radiation Detectors for Gamma-Ray Spectroscopy. *ACS Energy Letters*. 2022;7(3):1066-1085. doi:10.1021/acseenergylett.2c00031
- Roy UN, Camarda GS, Cui Y, Yang G, James RB. Impact of selenium addition to the cadmium-zinc-telluride matrix for producing high energy resolution X-and gamma-ray detectors. *Scientific Reports*. 2021;11(1). doi:10.1038/s41598-021-89795-z
- Smith MB, Bolotnikov A, Brown CA, et al. Performance Studies of Position-Sensitive Capacitive Frisch-Grid TLBR Detectors. In: *2020 IEEE Nuclear Science Symposium and Medical Imaging Conference, NSS/MIC 2020*. Institute of Electrical and Electronics Engineers Inc.; 2020. doi:10.1109/NSS/MIC42677.2020.9508036
- Feng Y, Pan L, Wei H, et al. Low defects density CsPbBr₃ single crystals grown by an additive assisted method for gamma-ray detection. *Journal of Materials Chemistry C*. 2020;8(33):11360-11368. doi:10.1039/d0tc02706e
- Kang J, Wang LW. High Defect Tolerance in Lead Halide Perovskite CsPbBr₃. *Journal of Physical Chemistry Letters*. 2017;8(2):489-493. doi:10.1021/acs.jpclett.6b02800
- Wei H, Desantis D, Wei W, et al. Dopant compensation in alloyed CH₃NH₃PbBr_{3-x}Cl_x perovskite single crystals for gamma-ray spectroscopy. *Nature Materials*. 2017;16(8):826-833. doi:10.1038/nmat4927
- He Y, Petryk M, Liu Z, et al. CsPbBr₃ perovskite detectors with 1.4% energy resolution for high-energy γ -rays. *Nature Photonics*. 2021;15(1):36-42. doi:10.1038/s41566-020-00727-1
- Meng LJ, He Z. Exploring the limiting timing resolution for large volume CZT detectors with waveform analysis. *Nuclear Instruments and Methods in Physics Research*,

- Section A: Accelerators, Spectrometers, Detectors and Associated Equipment. 2005;550(1-2):435-445. doi:10.1016/j.nima.2005.04.076
9. He Y, Petryk M, Liu Z, et al. CsPbBr₃ perovskite detectors with 1.4% energy resolution for high-energy γ -rays. *Nature Photonics*. 2021;15(1):36-42. doi:10.1038/s41566-020-00727-1
 10. Pan L, Feng Y, Huang J, Cao LR. Comparison of Zr, Bi, Ti, and Ga as Metal Contacts in Inorganic Perovskite CsPbBr₃ Gamma-Ray Detector. *IEEE Transactions on Nuclear Science*. 2020;67(10):2255-2262. doi:10.1109/TNS.2020.3018101
 11. Wang X, Li Y, Xu Y, et al. Ion Migrations in Lead Halide Perovskite Single Crystals with Different Halide Components. *Physica Status Solidi (B) Basic Research*. 2020;257(6). doi:10.1002/pssb.201900784
 12. Wang W, Wang X, Zhang B, Guo Y, Xu Q. Ion migration of MAPbBr₃ single crystal devices with coplanar and sandwich electrode structures. *Physica B: Condensed Matter*. 2020;593. doi:10.1016/j.physb.2020.412310
 13. Wang X, Li Y, Xu Y, et al. Ion Migrations in Lead Halide Perovskite Single Crystals with Different Halide Components. *Physica Status Solidi (B) Basic Research*. 2020;257(6). doi:10.1002/pssb.201900784
 14. Datta A, Becla P, Motakef S. Novel Electrodes and Engineered Interfaces for Halide-Semiconductor Radiation Detectors. *Scientific Reports*. 2019;9(1). doi:10.1038/s41598-019-46360-z
 15. Datta A, Fiala J, Becla P, Motakef S. Stable room-temperature thallium bromide semiconductor radiation detectors. *APL Materials*. 2017;5(10). doi:10.1063/1.5001181
 16. Datta A, Becla P, Motakef S. Visualization of TlBr ionic transport mechanism by the Accelerated Device Degradation technique. *Nuclear Instruments and Methods in Physics Research, Section A: Accelerators, Spectrometers, Detectors and Associated Equipment*. 2015;784:37-43. doi:10.1016/j.nima.2015.01.021
 17. He Y, Petryk M, Liu Z, et al. CsPbBr₃ perovskite detectors with 1.4% energy resolution for high-energy γ -rays. *Nature Photonics*. 2021;15(1):36-42. doi:10.1038/s41566-020-00727-1
 18. He Y, Kontsevoi OY, Stoumpos CC, et al. Defect Antiperovskite Compounds Hg₃Q₂I₂ (Q = S, Se, and Te) for Room-Temperature Hard Radiation Detection. *J Am Chem Soc*. 2017;139(23):7939-7951. doi:10.1021/jacs.7b03174
 19. Shah KS, Lund JC, Olschner F, Moy L, Squillante MR. Thallium bromide radiation detectors. *IEEE Transactions on Nuclear Science*. 1989;36(1):199-202. doi:10.1109/23.34434
 20. Toyama H, Higa A, Yamazato M, Maehama T, Ohno R, Toguchi M. Quantitative analysis of polarization phenomena in CdTe radiation detectors. *Japanese Journal of Applied Physics, Part 1: Regular Papers and Short Notes and Review Papers*. 2006;45(11):8842-8847. doi:10.1143/JJAP.45.8842
 21. Smith MB, Bolotnikov A, Brown CA, et al. Performance Studies of Position-Sensitive Capacitive Frisch-Grid TLBR Detectors. In: *2020 IEEE Nuclear Science Symposium and Medical Imaging Conference, NSS/MIC 2020*. Institute of Electrical and Electronics Engineers Inc.; 2020. doi:10.1109/NSS/MIC42677.2020.9508036
 22. Zhang B bin, Wang F, Zhang H, et al. Defect proliferation in CsPbBr₃ crystal induced by ion migration. *Applied Physics Letters*. 2020;116(6). doi:10.1063/1.5134108
 23. Kang J, Wang LW. High Defect Tolerance in Lead Halide Perovskite CsPbBr₃. *Journal of Physical Chemistry Letters*. 2017;8(2):489-493. doi:10.1021/acs.jpcclett.6b02800